Macromolecular Rapid Communications

Supporting Information

for *Macromol. Rapid Commun.*, DOI 10.1002/marc.202300724

Semi-Transparent Luminescent Solar Concentrators Based on Intramolecular Energy Transfer in Polyurethane Matrices

*Elisavet Tatsi, Matteo De Marzi, Luca Mauri, Alessia Colombo, Chiara Botta, Stefano Turri, Claudia Dragonetti and Gianmarco Griffini**

Supporting Information

Semi-transparent Luminescent Solar Concentrators based on Intramolecular Energy Transfer in Polyurethane Matrices

*Elisavet Tatsi, Matteo De Marzi, Luca Mauri, Alessia Colombo, Chiara Botta, Stefano Turri, Claudia Dragonetti, Gianmarco Griffini**

* Corresponding author E-mail: gianmarco.griffini@polimi.it

Table of Contents

S1 Characterization of the new compounds

S1.1 ^{1}H NMR of new Fluorescent Diols

4,7-di(4-formyl-phenyl)benzo[c][1,2,5]thiadiazole (**1**)

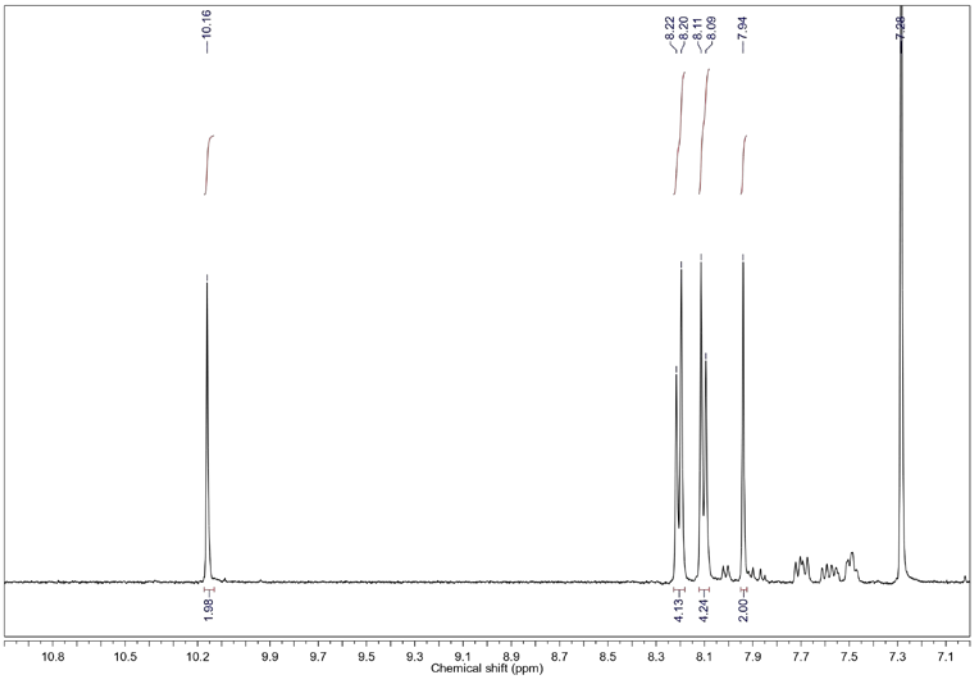

Figure S1. ^{1}H-NMR of compound **1**.

4,7-di(4-hydroxymethyl-phenyl)benzo[*c*][1,2,5]thiadiazole, **(bHPBT)**

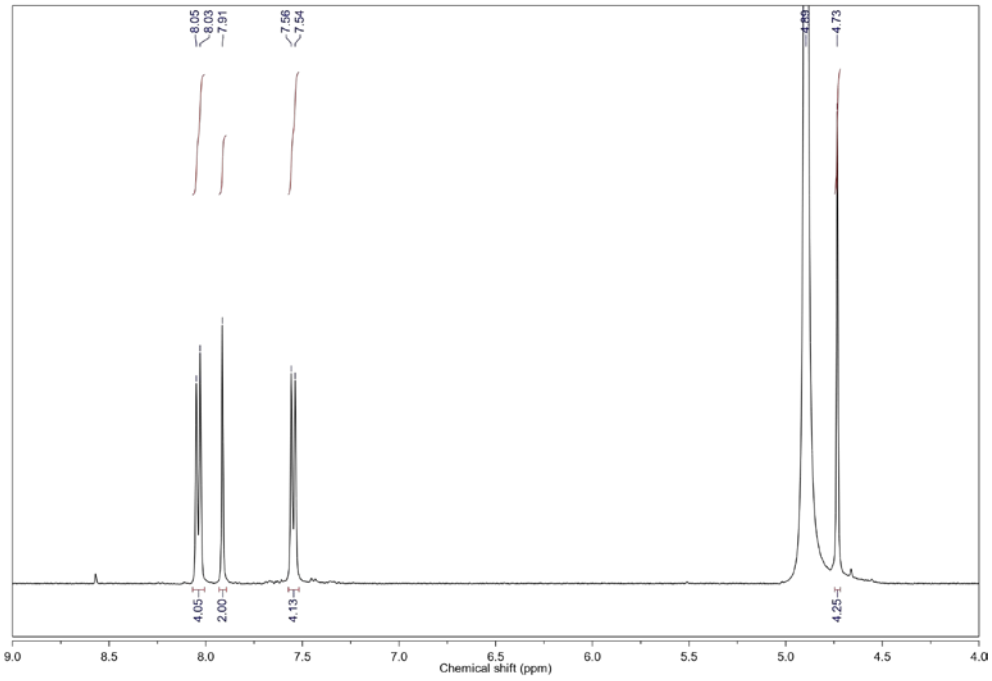

Figure S2. ^{1}H-NMR of compound **bHPBT**.

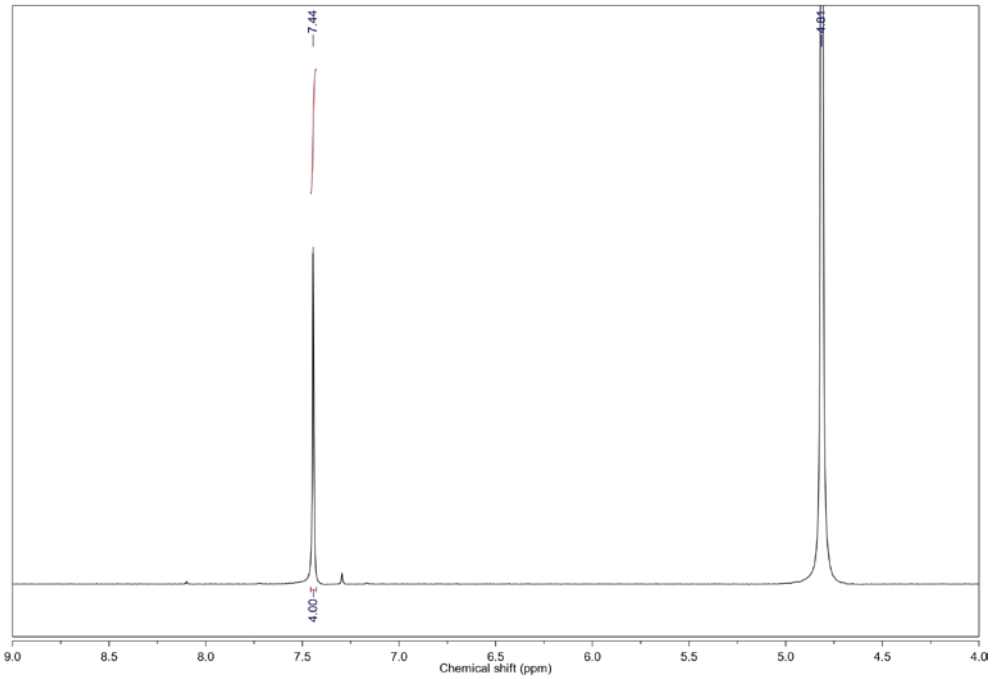

o

Figure S3. ^{1}H-NMR of compound **2**.

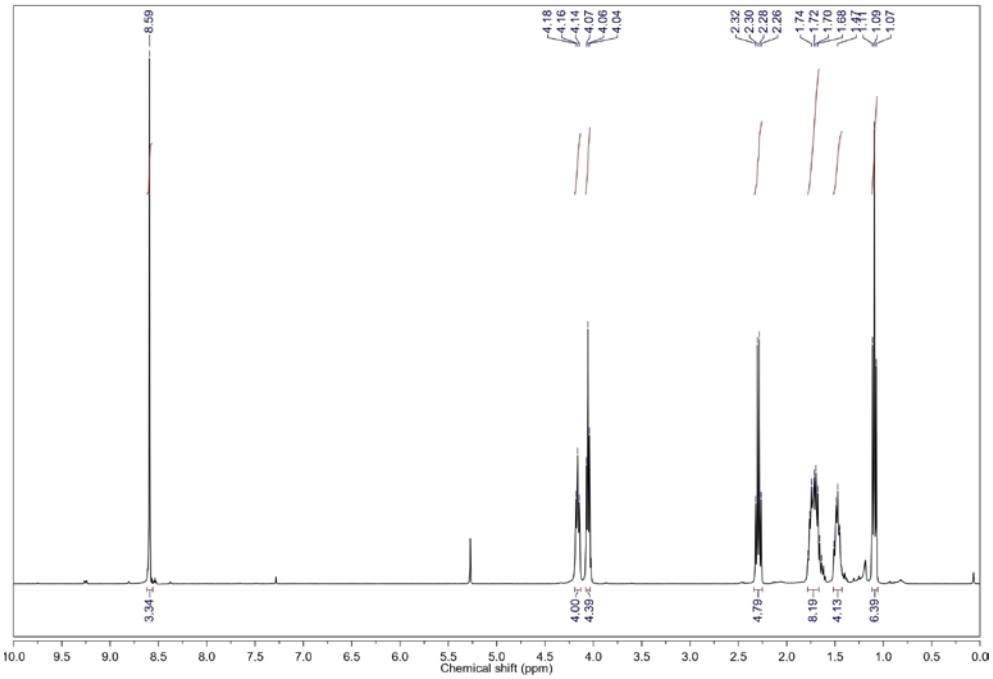

N

Figure S4. ^{1}H-NMR of compound **3**.

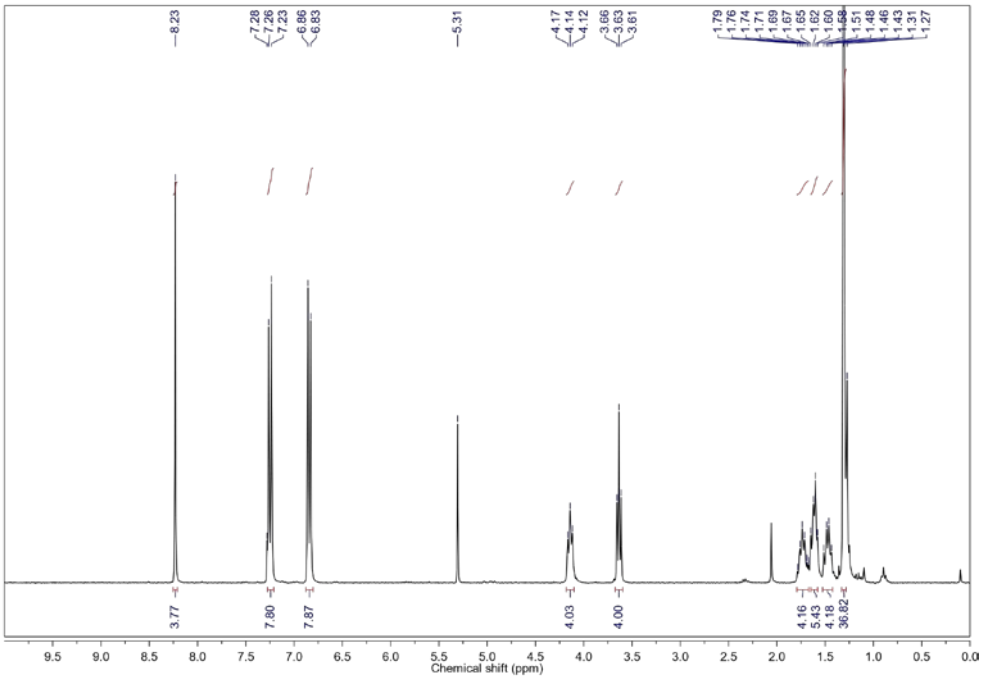

Figure S5. ^{1}H-NMR of compound bHPDI.

S2 Photophysical Characterization in Solution

The photophysical characterization of bHPBT and bHPDI was carried out at room temperature in methanol and in dichloromethane, respectively. Electronic absorption spectra were obtained with a Shimadzu UV3600 spectrometer and quartz cuvettes with 1 cm optical path length. Absolute luminescence quantum yields were measured with a C11347 Quantaurus Hamamatsu Photonics K.K Spectrometer equipped with a 150 W Xenon lamp, an integrating sphere, and a multichannel detector; the estimated error is 5%. Steady state and time-resolved fluorescence data were collected with a FS980 spectrofluorimeter (Edinburgh Instruments Ltd).

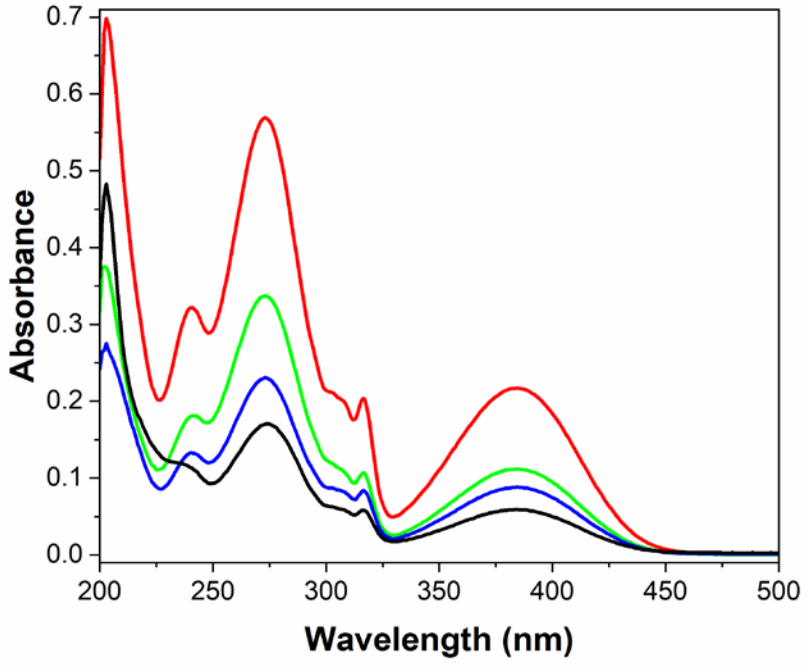

Figure S6. Absorption spectrum of bHPBT in MeOH: 5.0E-6 M (black curve), 7.5E-6 M (blue curve), 1.0E-5 M (green curve), 2.0E-5 M (red curve).

Table S1. Absorption maxima, absorbance, and molar extinction coefficients (ε) of bHPBT.

λ_{max} (nm)	Concentration (M)	Absorbance	ε (M^{-1} cm^{-1})
273	5.00E-06	0.16984	26582
	7.50E-06	0.23081	R^2 = 0.9891
	1.00E-05	0.33736	
	2.00E-05	0.56905	
384	5.00E-06	0.05876	10482
	7.50E-06	0.08796	R^2 = 0.9996
	1.00E-05	0.11171	
	2.00E-05	0.21703	

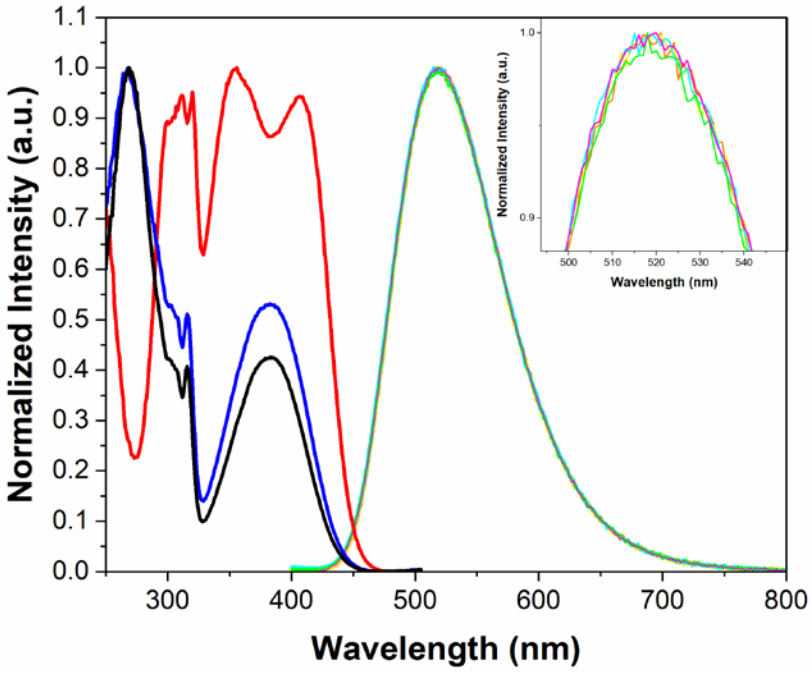

Figure S.7 Photoluminescence spectra of bHPBT in MeOH. Emission spectra: 1.4E-4 M, λex 384 nm (orange curve), 2.0E-5 M, λex 384 nm (yellow curve), 7.5E-6 M, λex 384 nm (pink curve), 7.5E-6 M, λex 316 nm (light-blue curve), 7.5E-6 M, λex 270 nm (green curve). Excitation spectra: 1.4E-4 M, λem 519 nm (red curve), 2.0E-5 M, λem 519 nm (blue curve), 7.5E-6 M, λem 519 nm (black curve).

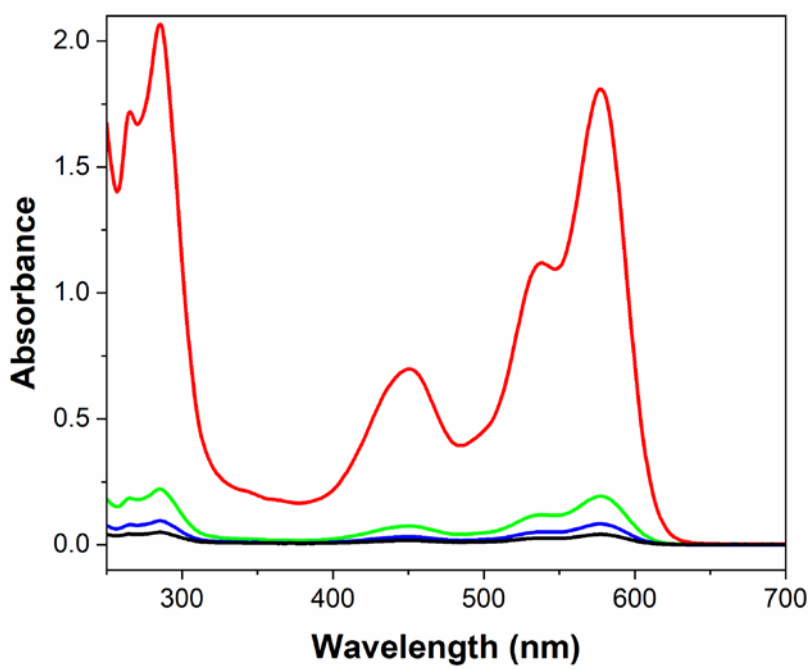

Figure S8. Absorption spectrum of bHPDI in dicholoromethane: 1.0E-6 M (black curve), 2.0E-6 M (blue curve), 5.0E-6 M (green curve), 5.0E-5 M (red curve).

Table S2. Absorption maxima, absorbance, and molar extinction coefficients (ε) of bHPDI.

λ_{max} (nm)	Concentration (M)	Absorbance	ε (M^{-1} cm^{-1})
285	1.00E-06	0.05019	
	2.00E-06	0.09533	41039
	5.00E-06	0.22165	R^2 = 0.9999
	5.00E-05	2.0645	
451	1.00E-06	0.01697	
	2.00E-06	0.03137	13889
	5.00E-06	0.07367	R^2 = 0.9999
	5.00E-05	0.69802	
538	1.00E-06	0.02565	
	2.00E-06	0.05092	22273
	5.00E-06	0.11876	R^2 = 0.9999
	5.00E-05	1.11914	
577	1.00E-06	0.04108	
	2.00E-06	0.08285	36007
	5.00E-06	0.19291	R^2 = 0.9999
	5.00E-05	1.80953	

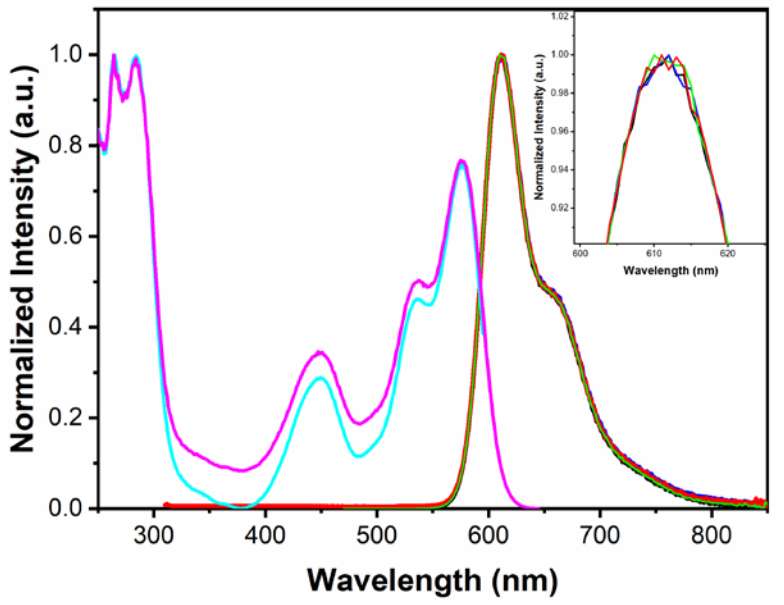

Figure S9. Photoluminescence spectra of bHPDI in dicholoromethane. Emission spectra: 2.0E-6 M, λ_{ex} 284 nm (red curve), 2.0E-6 M, λ_{ex} 450 nm (green curve), 2.0E-6 M, λ_{ex} 540 nm (black curve), 2.0E-6 M, λ_{ex} 576 nm (blue curve). Excitation spectra: 2.0E-6 M, λ_{em} 613 nm (light-blue curve), 2.0E-6 M, λ_{em} 666 nm (pink curve).

S3 Characterization of the Clear and Luminescent Polyurethane Systems

S3.1 Feed Compositions of Synthesized Polyurethanes

The feed compositions for all polyurethane material formulations are reported in Table S3.

Table S3. Mass feed of fluorescent diols (bHPBT, bHPDI) in mg.

	Sample	Donor bHPBT (mg)	Acceptor bHPDI (mg)
PU DONOR	***PU-D1***	20	-
	PU-D1.25	30	-
	PU-D1.5	40	-
PU ACCEPTOR	***PU-A0.1***	-	8.25
	PU-A0.2	-	17.5
	PU-A0.4	-	35
PU D-A	***PU-DA7.5***	40	8.25
	PU-DA15	40	17.5
	PU-DA30	40	35

S3.2 FTIR Analysis

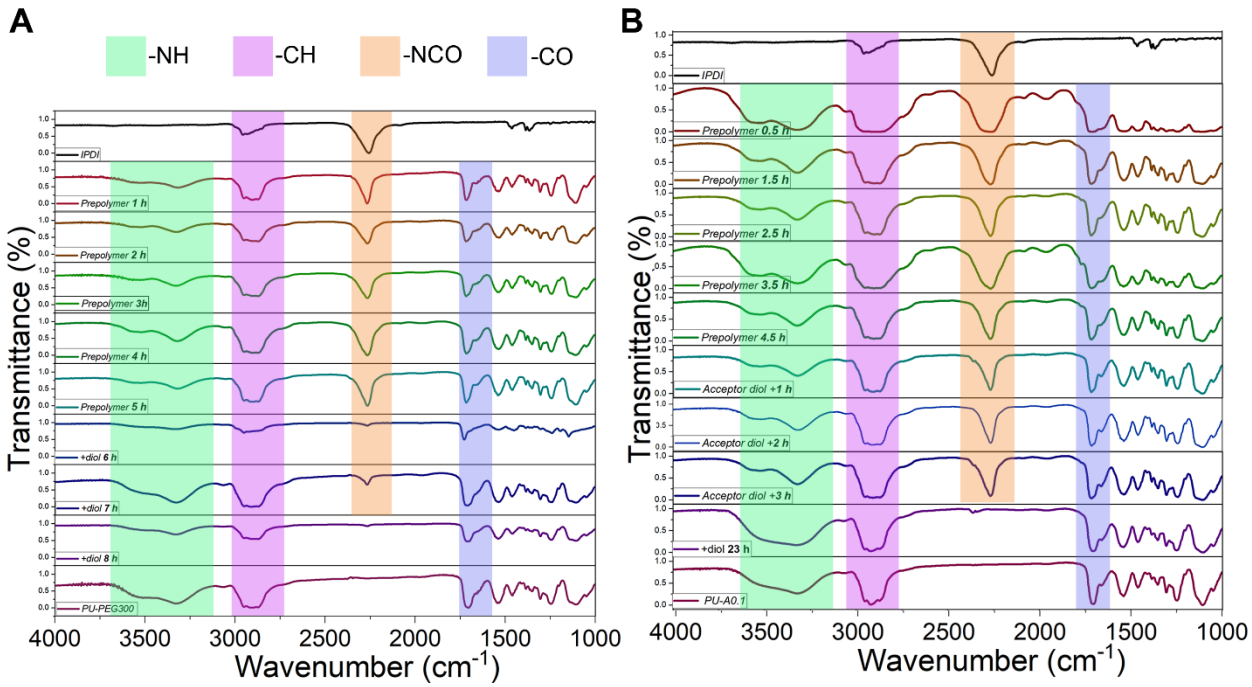

Figure S10. A) FTIR of clear *PU-PEG300*, B) FTIR of PU (PU-A0.1)

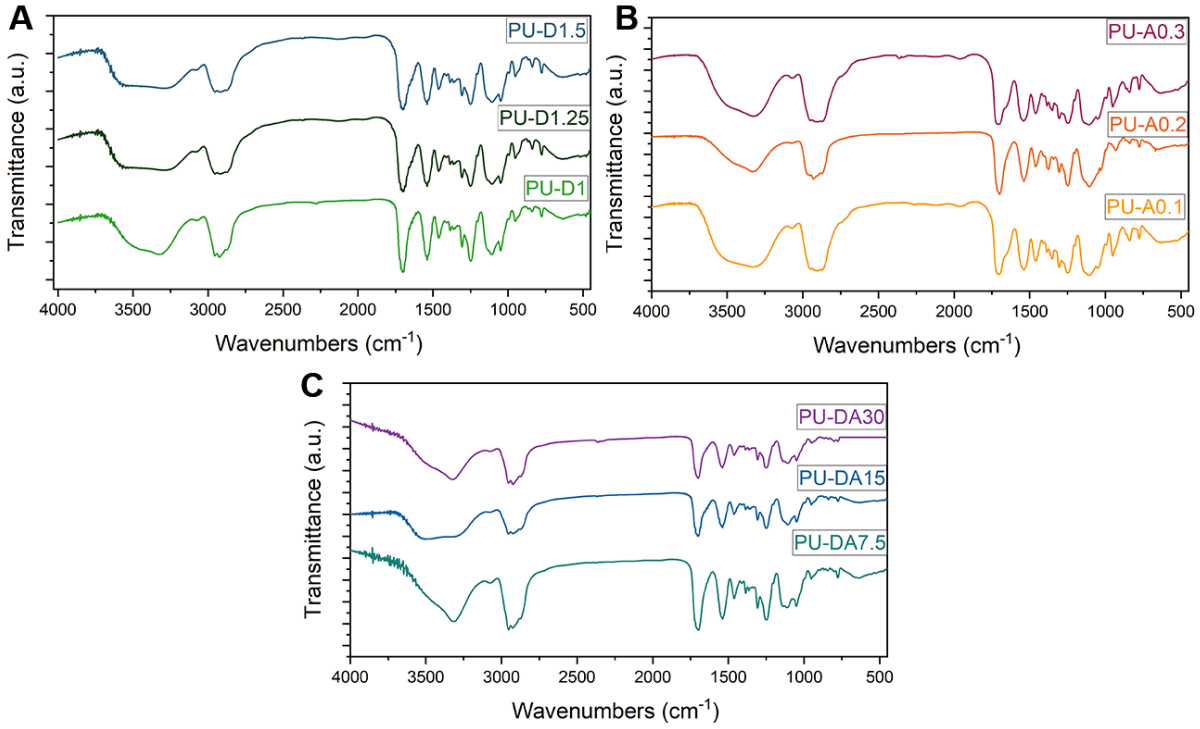

Figure S11. IR spectra of: A) series of donor polyurethanes (PU-D*x*), B) series of acceptor polyurethanes (PU-A*y*), C) series of donor-acceptor polyurethanes (PU-DA*z*)

S3.3 ^{1}H NMR of Luminescent Polyurethanes

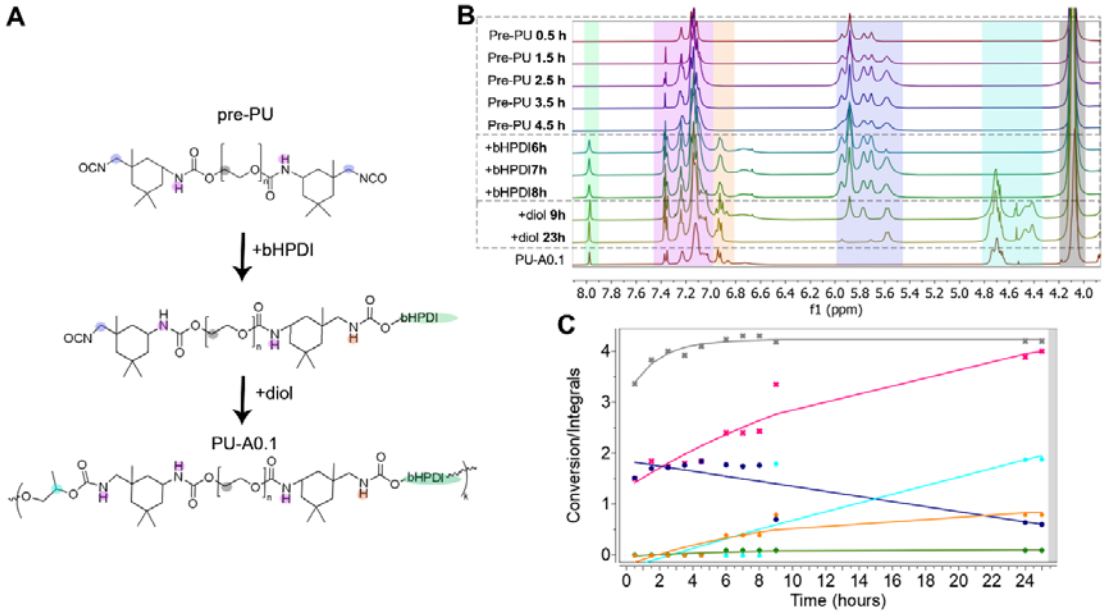

Figure S12. A) Formation of urethane bond by reaction between isophorone diisocynate and diol; B) Stacked plot of ^{1}H NMR data, during the progress of a representative reaction from 0.5 to 24 h of total reaction, including the formation of prepolymer and then the chain extension with first the bHPDI and then 1,2 propanediol for the final formation of the polyurethane; C) Trends of ^{1}H NMR spectra over reaction time based on integrated regions of interest.

S4 Thermal and Optical Characterization of Clear Polyurethanes

S4.1 DSCs of Clear Polyurethanes

Table S4: glass transition temperature (Tg) values of clear polyurethanes

Sample	Tg [°C]
PU-PEG300	10
PU-PEG600	0
PU-PEG1000	-15
PU-PEG2000	-20

S4.2 Transmittance of Clear Polyurethanes

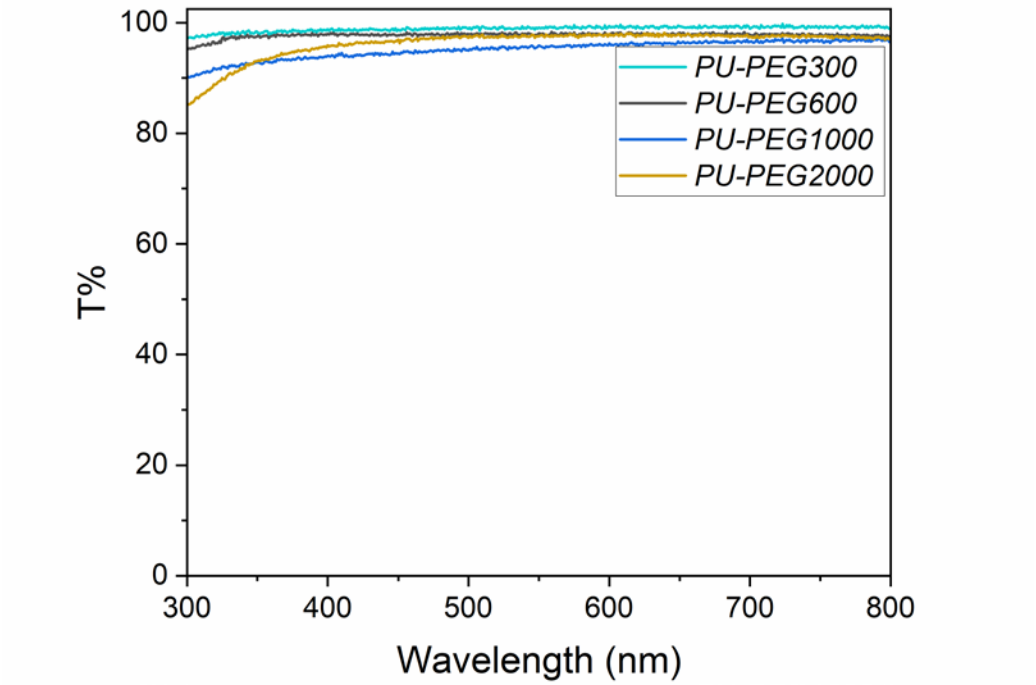

Figure S13. T% of clear Pus.

S.5 Photophysical Characterization of Polyurethanes

S5.1 Photophysical Characterization of PU-Dx, PU-Ay Polyurethanes

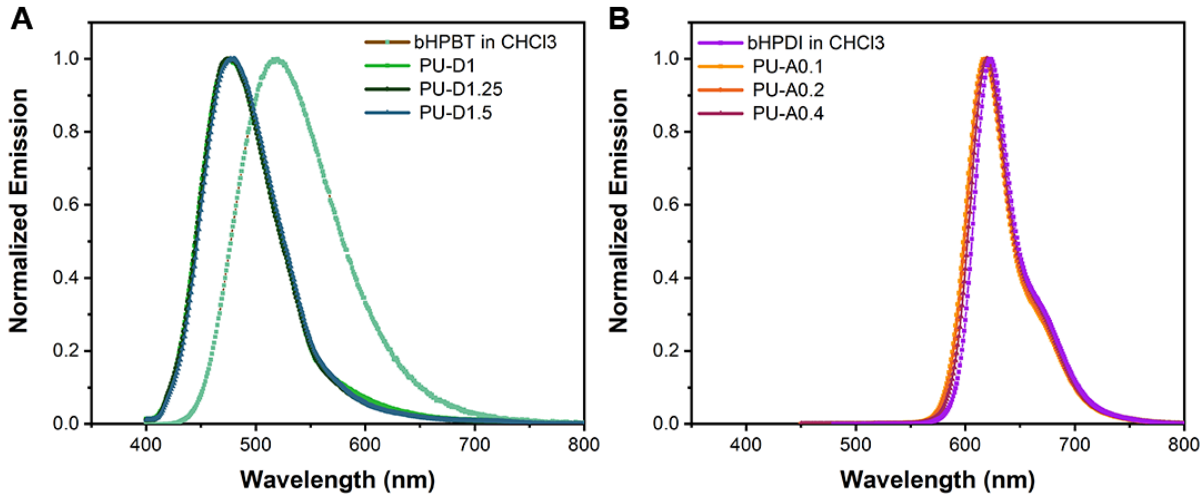

Figure S14. Emission of bHPBT donor in solution and front-face emission of PU-D1, PU-D1.25, PU-D1.5, B) Emission of bHPDI acceptor in solution and front-face emission of PU-A0.1, PU-A0.2, PU-A0.4

Table S5. Absorption and emissions of pristine dyes and PU systems.

	Absorbance	***Edge-emission***	***Front-face emission***	***Emission solution***
Sample	λ_{max} ***[nm]***	λ_{max} ***[nm]***	λ_{max} ***[nm]***	λ_{max} ***[nm]***
	273, 384			519
	285, 451, 538, 577			622
PU-D1	275, 386	479	476	
PU-D1.25	275, 386	480	477	
PU-D1.5	275, 386	481	477	
PU-A0.1	286, 450, 541, 580	610	616	
PU-A0.2	286, 450, 541, 580	616	617	
PU-A0.4	286, 450, 541, 580	624	619	
PU-DA7.5	278, 389, 540, 584	472, 612	477, 622	
PU-DA15	278, 389, 540, 584	474, 625	478, 629	
PU-DA30	278, 389, 540, 584	477, 636	478, 634	
BLEND-PU1	278, 389, 540, 584	472, 612	477, 622	
BLEND-PU2	278, 389, 540, 584	473, 622	477, 623	
BLEND-PU3	278, 389, 540, 584	473, 630	477, 625	

S5.2 Photophysical Characterization of BLEND-PU*n* Polyurethanes

To create the blends (BLEND-PU*n*), PU-D*1.5* and PU-A*y* polyurethanes were mechanically mixed with a solvent. The concentration of the final solution was determined to be 20% weight for uniform film formation. Three blends were prepared with dye ratios of 1:10, 2.5:10, and 5:10 of acceptor to donor. By keeping the solvent volume fixed at 1 mL of chloroform, the appropriate amounts of each polymer required to achieve the desired dye ratio were calculated. The masses of each polymer added to the blends are presented in Table S5.

Table S6. Molar and weight ratios of BLEND polyurethanes

Sample	Weight Ratio		Molar Ratio	
	Donor	Acceptor	Donor	Acceptor
Blend_PU1	10	1 (PU-A0.1)	0.0255	0.00169
Blend_PU2	10	2.5 (PU-A0.2)	0.0255	0.00337
Blend4_PU3	10	7 (PU-A0.4)	0.0255	0.00675

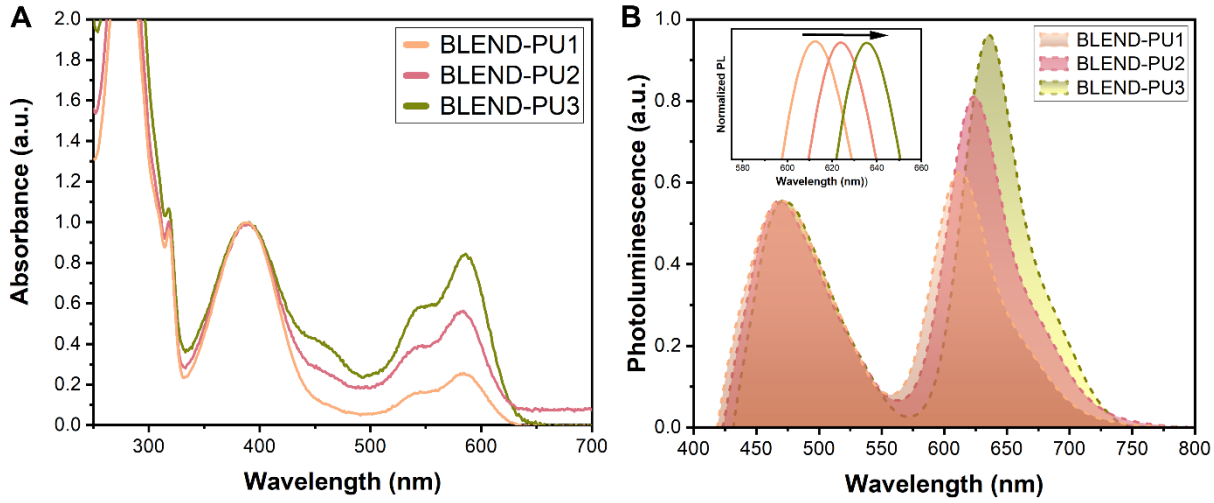

Figure S15. A) UV-Vis and B) fluorescence spectra of donor-acceptor polyurethane BLENDS excitation wavelength was set at 384 nm.

The solid-state absorption and emission behaviors of donor-acceptor polyurethane blends were examined in thin-film configuration, as illustrated in **Figure S16.** The absorption and fluorescence spectra of the three BLEND-PU*n* systems were investigated across varying bHPBT/bHPDI weight (molar) ratios, revealing a noticeable enhancement in both absorption and fluorescence intensity as the bHPDI (acceptor) content increased within the polyurethane blend formulation. Furthermore, the absorption and emission spectral profiles exhibited distinct features characteristic of bHPBT and bHPDI molecules, consistent with observations in copolymers (PU-DAz). Specifically, three absorption peak maxima were consistently observed

across all donor-acceptor polymers, centered at 279 nm, 387 nm, and 584 nm (Table S6). Additionally, the emission spectra depicted two prominent bands peaking at λmax = 470 nm and approximately λmax = 620-650 nm, matching well the fluorescence properties of copolymers series (PU-DA*z*).

S5.3. Transmission spectra of Polyurethane LSC systems

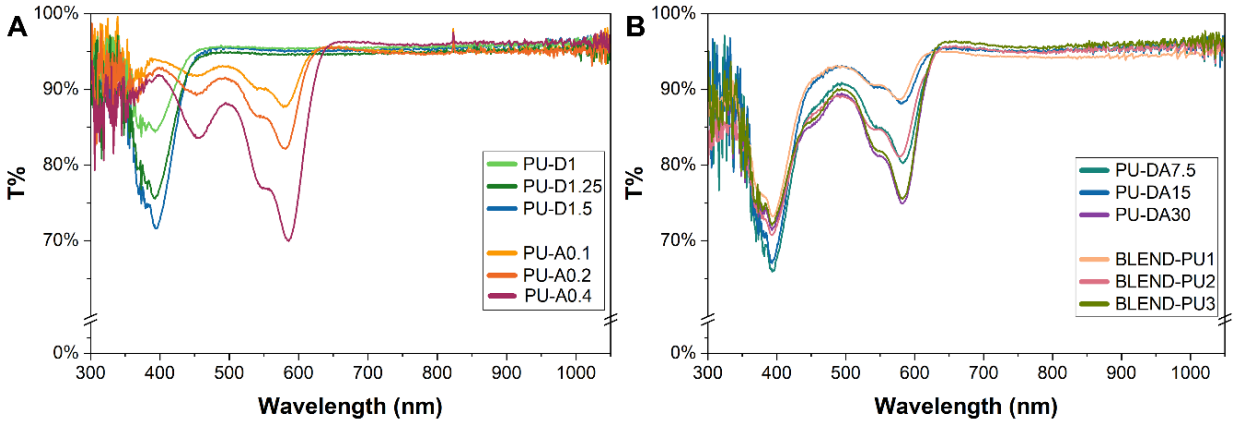

Figure S16. Transmission spectra of A) donor polyurethanes PUD*x* and acceptor polyurethanes PUD*y* and B) comparison of copolymer PU-DA*z* and Blend systems of PUD*x*-PUA*y*.

S6 Photophysical Characterization and Time-resolved Spectroscopy

The extent of spectral overlap *J* between donor (bHPBT) and acceptor (bHPDI) species was numerically evaluated according to the following equation: [S1,S2]

$$J = \lambda^4 \bar{I}_D\,(\lambda)\,\varepsilon_A(\lambda) \quad \text{(S1)}$$

Which is dependent on the acceptor molar absorptivity (or extinction coefficient) spectrum ε_A and the donor emission spectrum $\bar{I}_D$ normalized to unity: [S1]

$$\int \bar{I}_D\,(\lambda)\,d\lambda \quad \text{(S2)}$$

The fluorescence quantum yields of PU-D1 to PU-D1.5 are reported in **Table 2** showing a relative constant value with a proximity to ~100% in the solid state. When it comes to acceptor-only PUs (PU-A*y*), the fluorescence quantum yields are reducing with the increase of the acceptor (bHPDI) diol loading. Incorporating PDI directly into the backbone of the polymer was a strategy to reduce the aggregation of PDI molecules and minimize the aggregation-caused quenching (ACQ) effect. However, even with this approach, the fluorescence quantum yield may still be low due to other factors such as self-quenching or energy transfer to impurities or defects in the polymer matrix.[S3–S5] Self-quenching occurs due to the small Stokes shift of perylene based molecules producing effects particularly relevant in high-concentration systems. Another factor that may affect the fluorescence quantum yield is energy transfer to impurities or defects in the polymer matrix. [S6] The presence of these impurities or defects can create energy traps that compete with the radiative decay pathway, resulting in a decrease in fluorescence quantum yield. [S7]

To overcome these challenges, it may be necessary to optimize the synthesis of the polymer matrix to reduce the occurrence of self-quenching and minimize the presence of impurities or defects that can act as energy traps. Additionally, it may be necessary to carefully control the loading concentration of bHPDI in the polymer matrix to achieve optimal fluorescence properties while avoiding bHPDI microaggregation inducing the ACQ effect. [S3,S4] Indeed the analysis of the PU-A lifetimes as a function of concentration, suggests the presence of longer lived species in the more concentrated samples, that are consistent with excimer emission from PDI dimers or excimers.

The energy transfer efficiency (η_{ET}) was estimated from the relation:

$$E = 1 - \frac{\tau_{DA}}{\tau_D} \quad \text{(S3)}$$

Where τ_D and τ_{DA} are the fluorescence average lifetimes of the donor in the absence and in the presence of the acceptor, respectively. Very similar results were obtained from steady state measurements as:

$$\eta_{ET} = 1 - PL_{DA}/PL_D \quad \text{(S4)}$$

where PL_{DA} is the integrated donor emission intensity and PL_D is assumed to be equal to the total emission intensity $PL_D = PL$.

Time-resolved fluorescence measurements were carried out on PU-DA7.5, PU-DA15, PU-DA30 coatings to determine the composition giving the most favorable resonance energy transfer efficiency.

PLQY measurements of the films were performed by using a home-made integrating sphere according to the procedure reported elsewhere[S8] with NanoLog composed by a iH320 spectrograph equipped with a Synapse QExtra charge-coupled device, by exciting with a monochromated 450W Xe lamp or with a 405nm Thorlabs DL5146-101S laser diode with LDC205C controller. The spectra are corrected for the instrument response. Time-resolved TCSPC measurements are obtained with PPD-850 single photon detector module by exciting with DD-405L DeltaDiode Laser and analysed with the instrument Software DAS6. The two-exponential fits to the emission decay curve allowed to determine the average fluorescence lifetime τ, calculated according to the following equation:

$$\tau = \frac{\sum_i A_i t_i}{\sum_i A_i} \quad \text{(S5)}$$

where A_i and t_i are the 2-exponential fit parameters $\sum_i A_i \, exp(\frac{t}{ti})$.

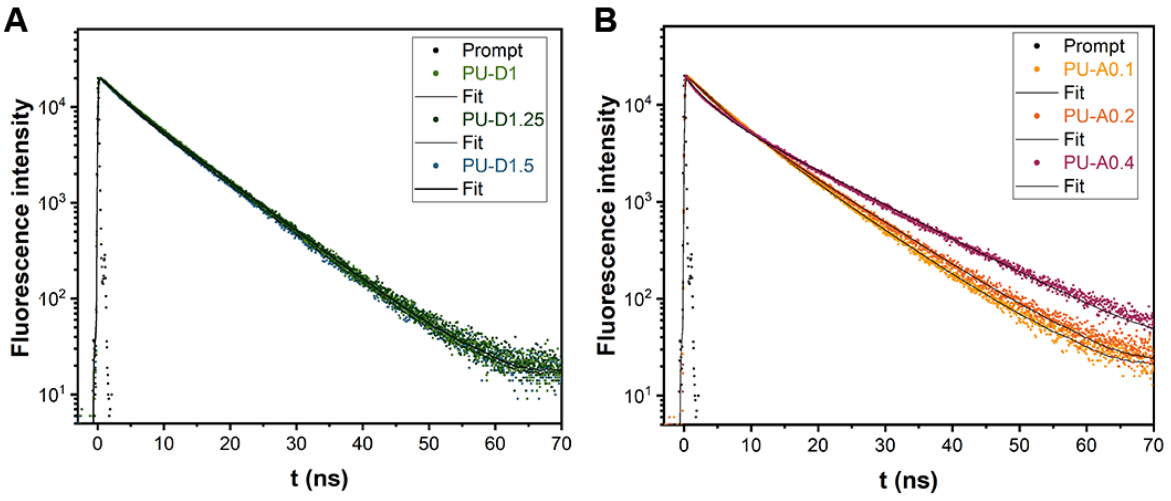

Figure S17. Emission decay (scatter plots) of PU-D*x* and PU-A*y* as cast film (λ_{exc}= 407 nm, λ_{em}=482 nm for PU-D's and λ_{em}=620-642 nm for PU-A's).

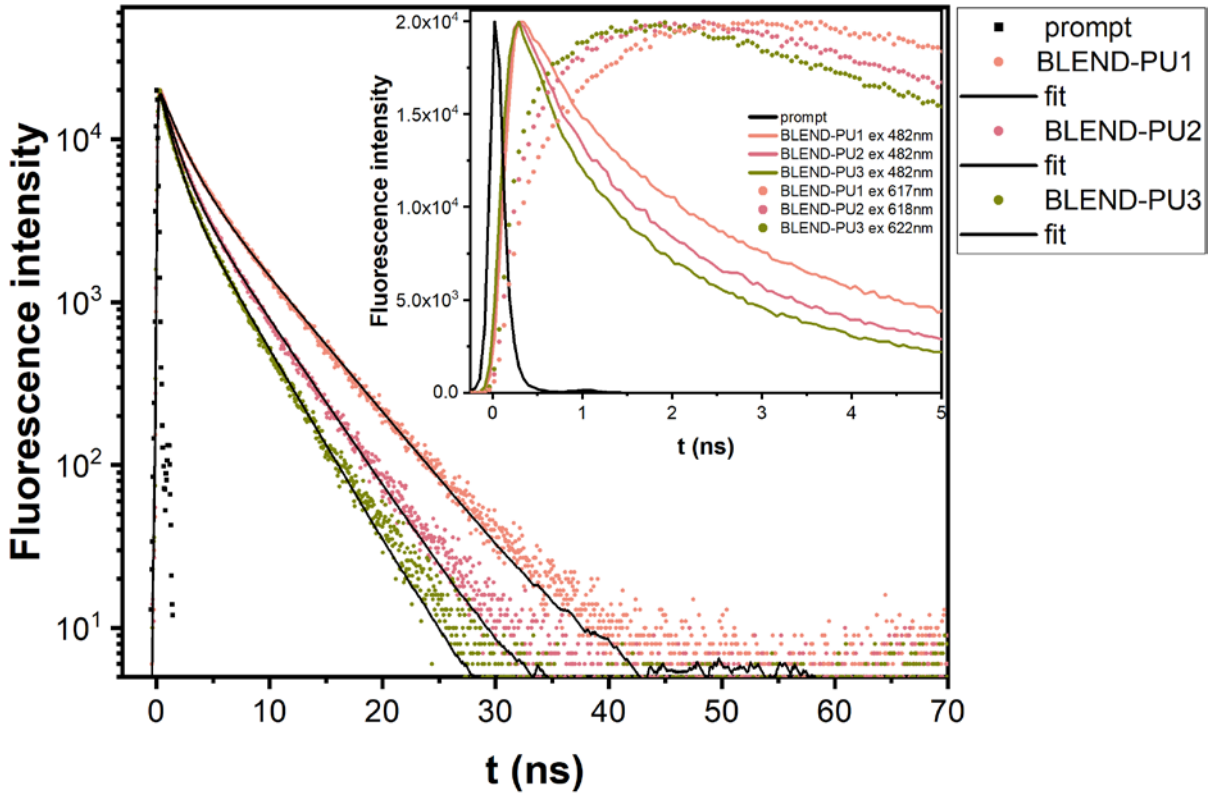

Figure S18. Emission decay (scatter plots) of BLENDS-PU*n* systems as cast film (excitation 407 nm, emission at 482 nm, solid lines are biexponential fits). In the inset an enlargement of the initial decay of BLEND-PU*n* systems is reported for emissions at 482 nm (donor, solid lines) and 617-618-622 nm (acceptor, dashed lines).

Table S7. Best fit parameters of two-exponential decays

Sample	A_1	t_1	A_2	t_2	χ^2
PU-D1	0.23	3.099446	0.77	8.434176	1.649227
PU-D1.25	0.23	2.946235	0.77	8.548127	1.621372
PU-D1.5	0.25	2.822848	0.75	8.411061	1.562442
PU-A0.1	0.89	6.402142	0.11	10.00968	1.989406
PU-A0.2	0.54	5.136543	0.46	9.869145	2.062477
PU-A0.4	0.44	3.905220	0.56	10.0322	3.065146
PU-DA7.5	0.68	0.874743	0.32	3.581776	3.380536
PU-DA15	0.76	0.481166	0.24	2.094583	4.965519
PU-DA30	0.79	0.437702	0.21	1.79591	3.219788
BLEND-PU1	0.58	1.602651	0.42	5.246365	1.948561
BLEND-PU2	0.65	1.250104	0.35	4.243445	2.413417
BLEND-PU3	0.68	1.06631	0.32	3.683018	2.478729

Table S8. Photophysical properties of the blends (BLEND-PU*n*) of luminescent polyurethanes: Fluorescence Efficiency (**Φ**); Fluorescence maximum position (λ^{max}); average lifetime of the donor in presence of the acceptor (τ_{DA}); Energy transfer efficiency (η_{ET}).

Sample	Φ[a] (5-10% error)	λ^{max} (nm)	λ^{max} (nm)	τ_{DA}[b] (ns)	η_{ET}[c]
BLEND_PU1	0.76	482	617	3.12	0.55
BLEND_PU2	0.71	482	618	2.29	0.67
BLEND_PU3	0.60	481	622	1.91	0.73

a) λ_{exc}=370nm; b) λ_{exc}=407nm, b) λ_{em}=482nm $\tau = \Sigma_i \alpha_i t_i$, from bi-exponential fits; c) η_{ET}= 1-τ_{DA}/τ_D with τ_D =7ns.

S7 Optical and Photovoltaic Characterization

S7.1 External and Internal Photon Efficiency

To characterize the optical performance of LSCs as photonic systems, two parameters were used, namely the external photon efficiency (η_{ext}) and the internal photon efficiency (η_{int}): [S9]

$$\eta_{ext} = \frac{N_{ph-out}}{N_{ph-in}} = \frac{Nº\ of\ edge\ emitted\ photons}{Nº\ of\ incident\ photons} = \frac{\sum_{i=1}^{4}\int_{300}^{800} P_{i(out)}(\lambda)\frac{\lambda}{hc}d\lambda}{\sum_{i=1}^{4}\int_{300}^{800} P_{(in)}(\lambda)\frac{\lambda}{hc}d\lambda} \quad \text{(S6)}$$

$$\eta_{int} = \frac{Nº\ of\ edge\ emitted\ photons}{Nº\ of\ absorbed\ photons} = \frac{\sum_{i=1}^{4}\int_{300}^{800} P_{i(out)}(\lambda)\frac{\lambda}{hc}d\lambda}{\sum_{i=1}^{4}\int_{300}^{800} P_{(in)}(\lambda)\frac{\lambda}{hc}(1-10^{-A(\lambda)})d\lambda} \quad \text{(S7)}$$

where $N_{ph\text{-}out}$ is the total number of edge-emitted photons summed over four edges (i = 1-4) of the LSC, $N_{ph\text{-}abs}$ is the total number of photons absorbed by the LSC, and $N_{ph\text{-}in}$ is the total number of photons incident on the top surface of the LSC. Also, h is Planck's constant (in J s) and c is the speed of light (in m s^{-1}). $N_{ph\text{-}out}$ is obtained from the sum of the output power spectra, $P_{i(out)}(\lambda)$, measured for each edge of the LSC (in W $nm^{-}1$), where λ is the wavelength of light (in nm). $P_{in}(\lambda)$ is the input power spectrum from the solar simulator incident on the top surface of the LSC (in W nm^{-1}).

Table S9. Average edge-emitted power output (from one edge) and corresponding total η_{ext} and η_{int} for all LSC systems, measured in the 300-800 nm wavelength range under AM1.5G 1000 W m^{-2} simulated sunlight (values averaged over four measures); maximum absorbance.

Sample	*Absorbance at λ_{max} 387 nm*	*Absorbance at λ_{max} 580 nm*	*Average single-edge power output [mW]*	η_{ext} [%]	η_{int} [%]
PU-D1	0.32	-	1.63 ± 0.18	0.85 ± 0.01	25.68 ± 1.32
PU-D1.25	0.47	-	3.58 ± 0.5	1.85 ± 0.008	38.05 ± 0.85
PU-D1.5	0.53	-	5.76 ± 0.32	2.91 ± 0.014	45.90 ± 1.21
PU-A0.1	-	0.29	3.88 ± 0.54	1.61± 0.005	47.94 ± 2.06
PU-A0.2	-	0.35	4.66 ± 0.39	2.44 ± 0.011	24.51 ± 1.73
PU-A0.4	-	0.68	6.72 ± 0.83	3.62 ± 0.005	23.66 ± 0.94
PU-DA7.5	0.58	0.24	6.81 ± 0.25	3.59 ± 0.015	37.27 ± 1.10
PU-DA15	0.58	0.41	7.44 ± 0.36	3.97 ± 0.008	33.15 ± 0.98
PU-DA30	0.57	0.48	6.99 ± 0.39	3.69 ± 0.013	27.79 ± 1.21
BLEND-PU1	0.51	0.19	4.59 ± 0.18	2.24 ± 0.022	33.10 ± 1.05
BLEND-PU2	0.51	0.38	6.39 ± 0.34	3.65 ± 0.005	30.75 ± 1.40
BLEND-PU3	0.51	0.45	5.21 ± 0.19	3.6 ± 0.014	26.52 ± 0.85

S7.2 Radiative overlap (RO)

To comprehensively understand the impact and extent of reabsorption losses on the performance of LSC devices, we conducted an evaluation of the radiative overlap (RO) as a function of the increase of acceptor content. This parameter provides insight into the likelihood of reabsorption processes occurring relative to dye loading. The RO quantifies the fraction of emitted light susceptible to reabsorption by the dye itself. It is calculated using the equation S8: [S10]

$$RO = \frac{\int Em(\lambda)[1 - T(\lambda)]d\lambda}{\int Em(\lambda)d\lambda} \cdot 100 \quad \text{(S8)}$$

where Em(λ) is the emission spectrum, [1-T(λ)] the fraction of absorbed light and T(λ) is the transmission spectrum obtained through UV-vis absorption measurements. RO should be as small as possible to ensure minimum reabsorption (RO → 0 for an emitter with perfectly non-overlapping absorption and emission spectra). As depicted in Figure S19, we observed a gradual increase in RO with increasing acceptor concentration. For instance, in the PU-DA7.5 system, a spectral overlap of 18% was recorded. This value progressively increased with higher acceptor concentrations, reaching approximately 24% (e.g., PU-DA15) and 31% (e.g., PU-DA15). It is essential to emphasize that while this approach is commonly used for evaluating single-dye systems in LSC devices, its accuracy may be limited in systems utilizing FRET principles due to the complex energy transfer dynamics involved.

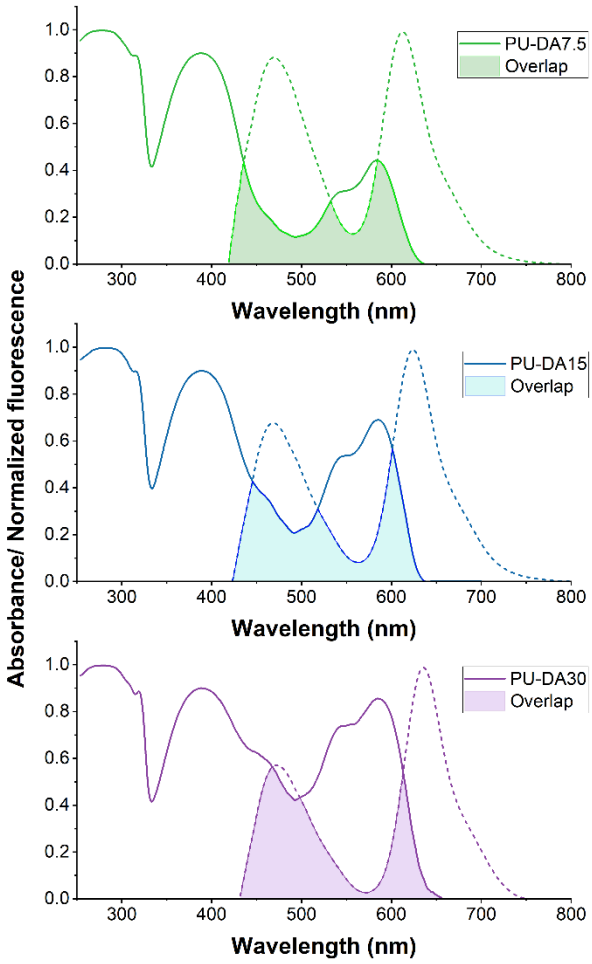

Figure S19. Absorption (1–T(λ)) and normalized emission spectra of PU-DAz systems.

S8 Power Conversion Efficiency of LSC-PV PU Systems

The power conversion efficiency (η_{dev}) was determined as the electrical power effectively extracted from the PV cells coupled with the LSC edges (P_{el}^{out}) relative to the optical input power hitting the top surface of the LSC (P_{opt}^{in}t), as reported in Equation S10:

$$\eta_{dev} = \frac{P_{el}^{out}}{P_{opt}^{in}} = \frac{I_{SC} V_{OC} FF}{P_{opt}^{in} A_{LSC}} \quad \text{(S9)}$$

where FF, I_{SC} and V_{OC} are the fill factor, the short-circuit current and the open-circuit voltage of the edge-coupled PV cells, respectively, P_{opt}^{in} is the incident solar power density (in mW cm^{-2}) and A_{LSC} is the front illuminated area of the LSC device (in cm^2). Because in this work two out of four edges of the LSC waveguide were coupled to PV cells, the overall η_{dev} (i.e., the power conversion efficiency for the LSC-PV assembly in which all four edges are couple with PV cells connected in series) can be achieved by multiplying η_{dev} by a factor 2.

The I-V curve and EQE of the mc-Si solar cells are presented below.

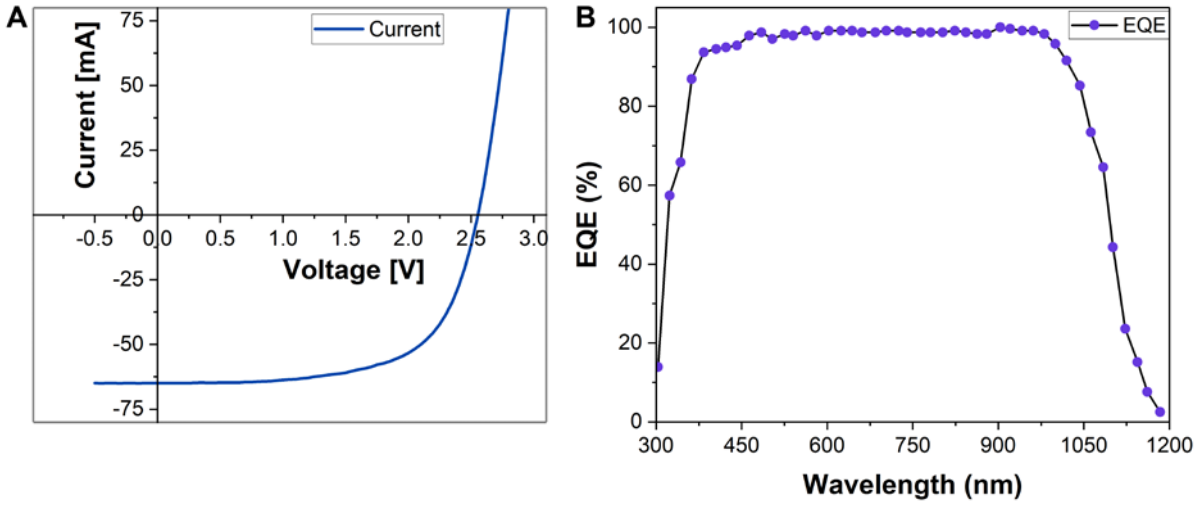

Figure S20. A) I-V curve and B) EQE of mc-Si solar cells used in this work.

Table S10. V_{OC}, I_{SC}, FF, P_{max} and η_{dev} calculated for donor-only (PU-D*x*), acceptor-only (PU-A*y*) and donor-acceptor (PU-DAz) LSC-PV assemblies.

Sample	$\mathbf{V_{OC}}$ **[V]**	$\boldsymbol{I_{SC}}$ **[mA]**	***FF***	$\mathbf{P_{max}}$ **[mW]**	$\boldsymbol{\eta_{dev}}$ **[%]**
PU-D1	2.13 ± 0.11	7.17 ± 0.79	0.57 ± 0.02	15.27 ± 0.82	0.45 ± 0.03
PU-D1.25	2.15 ± 0.28	7.19 ± 0.88	0.58 ± 0.06	15.46 ± 1.11	0.46 ± 0.07
PU-D1.5	2.22 ± 0.13	7.28 ± 0.79	0.61 ± 0.07	16.16 ± 0.77	0.51 ± 0.09
PU-A0.1	2.04 ± 0.38	7.30 ± 0.75	0.60 ± -0.07	14.89 ± 1.20	0.46 ± 0.08
PU-A0.2	2.10 ± 0.22	8.10 ± 0.98	0.59 ± 0.08	17.01 ± 0.85	0.52 ± 0.07
PU-A0.4	1.90 ± 0.05	8.28 ± 0.85	0.61 ± -0.05	15.73 ± 0.87	0.50 ± 0.11
PU-DA7.5	2.10 ± 0.25	8.13 ± 0.89	0.60 ± 0.08	17.07 ± 1.14	0.53 ± 0.05
PU-DA15	2.27 ± 0.29	8.98 ± 0.78	0.61 ± 0.09	20.36 ± 1.11	0.64 ± 0.07
PU-DA30	1.99 ± 0.17	8.37 ± 0.72	0.59 ± 0.07	16.66 ± 0.89	0.51 ± 0.03
BLEND-PU1	2.14 ± 0.18	7.58 ± 0.75	0.60 ± 0.08	16.22 ± 1.15	0.50 ± 0.05
BLEND-PU2	2.20 ± 0.27	8.01 ± 0.76	0.61 ± 0.09	17.62 ± 1.02	0.56 ± 0.07
BLEND-PU3	2.13 ± 0.09	7.97 ± 0.55	0.57 ± 0.06	16.97 ± 0.87	0.50 ± 0.01

S9 Average Visible-light Transmissivity (AVT) and Light Utilization Efficiency (LUE) of LSC PU Systems

The average visible-light transmissivity (AVT), a figure of merit particularly useful in describing the transmissivity of the devices mediated with the photopic response of the human eye, was also evaluated for all donor-acceptor PU-DA based LSCs. LSCs with a high AVT are desirable for applications of aesthetic relevance (e.g., buildings), since it indicates a device almost transparent to the human eye under sunlight illumination (thus, no or little alteration of incoming light).

The AVT was calculated with the following formula: [S11]

$$AVT\% = \frac{\int T\%\,(\lambda)\,P(\lambda)\,S(\lambda)d\lambda}{\int P(\lambda)\,S(\lambda)d\lambda} \qquad \text{(S10)}$$

where T%(λ) is the transmissivity of the device, measured with a UV-Vis spectrometer, P(λ) is the photopic response of the human eye to light (i.e., the curve that describes which wavelengths are the cone cells most sensible to), and S(λ) is the AM 1.5G solar spectrum expressed as photon flux in $cm^{-2}s^{-1}$.

The product of AVT and η_{dev} gives the Light Utilization Efficiency (LUE):

$$LUE = AVT \cdot \eta_{dev} \qquad \text{(S11)}$$

which represents a more appropriate and holistic measure for comparing different devices in view of their applicability as transparent PV systems.

Values of AVT and LUE for all PU-DA based LSC systems investigated in this work are reported in **Figure 5** in the main text. A comparison between BLEND-Pun and PU-DAz systems is shown in the figure below.

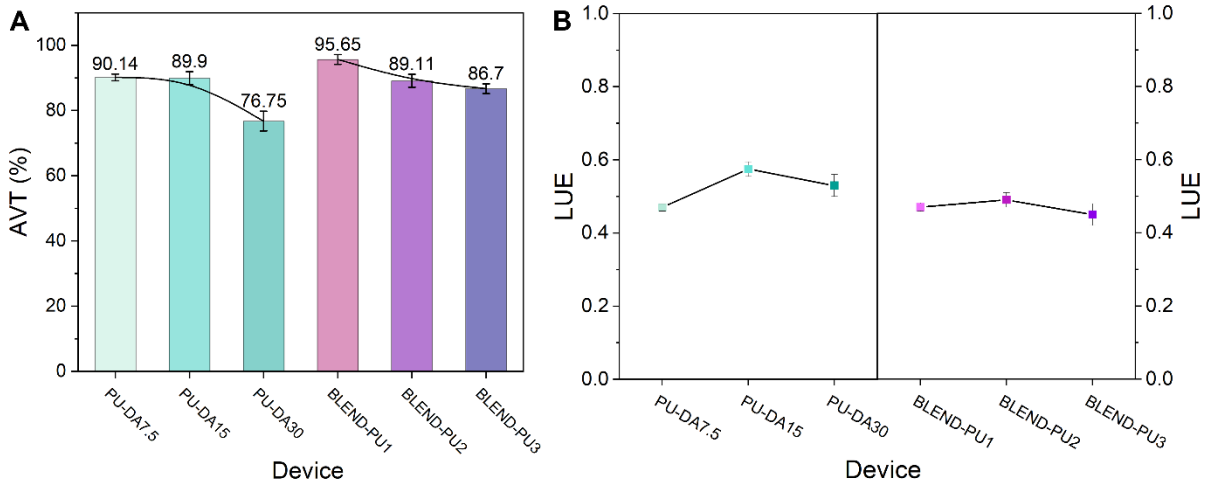

Figure S21. A) Average Visible Transmission (AVT) and B) Light Utilization Efficiency (LUE), for PU-DA based LSC devices comparison between co-polymers PU-DA*z* and BLEND-PU*n*

References

[S1] N. Hildebrandt, in *FRET – Förster Reson. Energy Transf.*, Wiley, **2013**, pp. 105–163.

[S2] J. R. Lakowicz, *Principles of Fluorescence Spectroscopy, Third Ed.*, Springer, Baltimore, **2000**.

[S3] A. Miasojedovas, K. Kazlauskas, G. Armonaite, V. Sivamurugan, S. Valiyaveettil, J. V. Grazulevicius, S. Jursenas, *Dye. Pigment.* **2012**, *92*, 1285.

[S4] Y. Hong, J. W. Y. Lam, B. Z. Tang, *Chem. Soc. Rev.* **2011**, *40*, 5361.

[S5] B. M. Squeo, F. Bertini, G. Scavia, M. Uslenghi, E. Fois, M. Pasini, C. Botta, *Dye. Pigment.* **2022**, *204*, 110473.

[S6] J. B. Birks, *J. Res. Natl. Bur. Stand. Sect. A Phys. Chem.* **1976**, *80A*, 389.

[S7] J. L. Banal, H. Soleimaninejad, F. M. Jradi, M. Liu, J. M. White, A. W. Blakers, M. W. Cooper, D. J. Jones, K. P. Ghiggino, S. R. Marder, T. A. Smith, W. W. H. Wong, *J. Phys. Chem. C* **2016**, *120*, 12952.

[S8] J. Moreau, U. Giovanella, J. P. Bombenger, W. Porzio, V. Vohra, L. Spadacini, G. Di Silvestro, L. Barba, G. Arrighetti, S. Destri, M. Pasini, M. Saba, F. Quochi, A. Mura, G. Bongiovanni, M. Fiorini, M. Uslenghi, C. Botta, *ChemPhysChem* **2009**, *10*, 647.

[S9] M. G. Debije, R. C. Evans, G. Griffini, *Energy Environ. Sci.* **2021**, *14*, 293.

[S10] D. Alonso-Álvarez, D. Ross, E. Klampaftis, K. R. McIntosh, S. Jia, P. Storiz, T. Stolz, B. S. Richards, *Prog. Photovoltaics Res. Appl.* **2015**, *23*, 479

[S11] C. J. Traverse, R. Pandey, M. C. Barr, R. R. Lunt, *Nat. Energy* **2017**, *2*, 849.